Journal of Hazardous Materials 166 (2009) 138–143

Contents lists available at ScienceDirect

Journal of Hazardous Materials

journal homepage: www.elsevier.com/locate/jhazmat

# Enhancement of titania by doping rare earth for photodegradation of organic dye (Direct Blue)

Zeinhom M. El-Bahy [b], Adel A. Ismail [a,*], Reda M. Mohamed [a]

[a] Advanced Materials Department, Central Metallurgical R and D Institute, CMRDI, P.O. Box 87 Helwan, Cairo, Egypt
[b] Department of Chemistry, Faculty of Science, Al-Azhar University, Nasr City 11884, Cairo, Egypt

ARTICLE INFO

*Article history:*
Received 23 June 2008
Received in revised form
12 September 2008
Accepted 5 November 2008
Available online 18 November 2008

*Keywords:*
$TiO_2$
Lanthanides
Photocatalysis
Direct Blue 53

ABSTRACT

Lanthanide ions ($La^{3+}$, $Nd^{3+}$, $Sm^{3+}$, $Eu^{3+}$, $Gd^{3+}$, and $Yb^{3+}$)/doped $TiO_2$ nanoparticles were successfully synthesized by sol–gel method. Their photocatalytic activities were evaluated using Direct Blue dye (DB53) as a decomposition objective. The structural features of $TiO_2$ and lanthanide ions/$TiO_2$ were investigated by XRD, SEM, UV-diffuse reflectance, and nitrogen adsorption measurements. Our findings indicated that XRD data characteristic anatase phase reflections and also XRD analysis showed that lanthanides phase was not observed on Lanthanide ions/$TiO_2$. The results indicated that $Gd^{3+}/TiO_2$ has the lowest bandgap and particle size and also the highest surface area and pore volume ($V_p$) as well. Lanthanide ions can enhance the photocatalytic activity of $TiO_2$ to some extent as compared with pure $TiO_2$ and it was found that $Gd^{3+}/TiO_2$ is the most effective photocatalyst. The photocatalytic tests indicate that at the optimum conditions; illumination time 40 min, pH ~4, 0.3 g/L photocatalyst loading and 100 ppm DB53; the dye removal efficiency was 100%. Details of the synthesis procedure and results of the characterization studies of the produced lanthanide ions/$TiO_2$ are presented in this paper.



## 1. Introduction

During the recent decades, the photocatalytic application using semiconductors has been received much attention to solve the environmental problems [1–4]. $TiO_2$ has turned out to be the semiconductor with the highest photocatalytic activity, being non-toxic, stable in aqueous solution and relatively inexpensive [5]. The photocatalytic property of $TiO_2$ is due to its wide bandgap and long lifetime of photogenerated holes and electrons. The high degree of recombination of the photo generated electrons and holes are a major limiting factor controlling its photocatalytic efficiency and impeding the practical application of these techniques in the degradation of contaminants in water and air. Thus, a major challenge in heterogeneous photocatalysis is the need to increase the charge separation efficiency of the photocatalysts [6].

Although $TiO_2$ is the most widely used photocatalyst, attention has been paid to metal ions-doped titania and testing their efficiency to replace pure $TiO_2$ and enhance the photocatalytic conversions. In order to decrease the bandgap of parent titania photocatalyst ($E_g$ = 3.2 eV), slow down the recombination rate of the $e^-/h^+$ pairs and enhance interfacial charge-transfer efficiency, the properties of $TiO_2$ have been modified by selective surface treatments such as surface chelation, surface derivatization, platinization, and by selective metal ions doping $TiO_2$ [7]. Coupled semiconductor photocatalysts exhibited a very high photocatalytic activity for both gas and liquid phase reactions. Researchers had much interest in coupling two semiconductor particles with different bandgap widths such as $TiO_2$–CdS, $TiO_2$–$WO_3$, $TiO_2$–$SnO_2$ [8], $TiO_2$–$MoO_3$ [9] $TiO_2$–$SiO_2$ [10] and $TiO_2$–$Fe_2O_3$ [11,12].

Lanthanide ions are known for their ability to form complexes with various Lewis bases e.g. acids, amines, aldehydes, alcohols, thiols, etc) in the interaction of these functional groups with the f-orbitals of the lanthanides. Particularly, $La^{3+}$, $Nd^{3+}$, $Sm^{3+}$, $Eu^{3+}$, $Gd^{3+}$, and $Yb^{3+}$(RE) –modified $TiO_2$ nanoparticles become of current importance for maximizing the efficiency of photocatalytic reactions, increase the stability of anatase phase and prevent the segregation of $TiO_2$ [13–17]. Thus, incorporation of lanthanide ions into a $TiO_2$ matrix could provide a means to concentrate on the organic pollutant at the semiconductor surface and consequently enhance the photoactivity of titania [16–20]. It was reported in literature that the optimum level of RE-doping is 1–2% to hinder the crystal growth of titania during calcination [15]. Although doping of lanthanide ions into $TiO_2$ attracted some attentions [21–26], such works are little so far.

The potential toxicity of some azo dyes has long been known. Disazo dyes based on benzidine are known to be carcinogenic [27,28]. Many papers on the relation between structure and carcinogenicity of azo dyes have been published [27]. Direct dyes are

* Corresponding author. Tel.: +20 2 25010643; fax: +20 2 25010639.
*E-mail address:* adelali11@yahoo.com (A.A. Ismail).

0304-3894/$ – see front matter © 2008 Elsevier B.V. All rights reserved.
doi:10.1016/j.jhazmat.2008.11.022

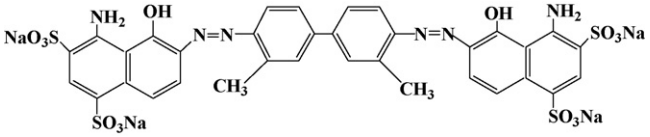

**Scheme 1.** Structure of Direct Blue 53 dye.

the compounds able to dye cellulose fibers (cotton, viscose, etc.) without the aid of mordants. Direct dyes constitute about 17% of all dyes used for dyeing textiles and about 30% of the dyes used for dyeing cellulose fibers [29]. A direct dye (sodium salt of a sulfonic acid) is anionic and soluble in water. According to its structure (Scheme 1) Direct Blue is a diazo dye based on benzidine.

Methods of decolorization have become important. In principle, decoloration is possible with one or more of the following methods: adsorption, coagulation, biodegradation, chemical degradation, and photodegradation [27]. For adsorption, activated charcoal, silica gel, bauxite, peat, wood, cellulose derivatives, and ion-exchange resins have been used, but these processes are in most cases not economically feasible [27].

In this contribution, we presented the influence of doping lanthanide ions (1 wt%) into $TiO_2$ and explored the role of surface area, surface texture, and bandgap energy on photocatalytic oxidation of Direct Blue 53 dye. Moreover, the removal of one of the organic pollutants (namely Direct Blue 53 dye) was investigated as a pattern of organic pollutant to evaluate the relative photocatalytic activity of the prepared photocatalyst samples.

## 2. Experimental

### 2.1. Materials

Titanium isopropoxide, Ytterbium(III) nitrate tetrahydrate, Neodymium nitrate hexahydrate, Samarium nitrate hexahydrate, Europium acetate tetrahydrate, Gadolinium(III) oxide and Lanthanum nitrate hexahydrate were used as precursors in the sol–gel syntheses. Direct Blue 53 (DB53), (molecular formula = $C_{34}H_{24}N_6Na_4O_{14}S_4$, molecular weight = 960.81), Scheme 1, was used.

### 2.2. Synthesis of the photocatalysts

The parent $TiO_2$ and lanthanide ions-doped $TiO_2$ nanoparticles were prepared by sol–gel technique. The sol corresponds to the overall molar ratio of $Ti(C_4H_9O_4):C_2H_5OH:H_2O:HNO_3$ = 1:20:4:0.001. $Ti(C_4H_9O_4)$ was first dissolved in ethanol to form titania sol; the lanthanide salts were dissolved into stoichiometric amount of water and nitric acid and then added drop wise into the titania sol through stirring for 30 min at room temperature. The prepared sol was left to stand for the formation of gel and dried at 120 °C. Finally, the obtained gel was calcined at 550 °C for 5 h to keep the lanthanide ions–$TiO_2$ in the anatase phase that has high photoactive sites. The atomic ratio of $TiO_2$:lanthanide ions was kept as 99:1 for all samples.

### 2.3. Characterization

X-ray powder diffraction (XRD) patterns were taken at room temperature using a model Bruker axs, D8 Advance. Average crystallize size ($D$) of the obtained powders were calculated by X-ray line broadening technique performed on the direction of lattice using computer software based on the so-called Hall-equation–Scherer's formula $D = 0.89\lambda/\beta\cos\theta$ [30], where $D$ is the crystallite size, $\lambda$ represents the X-ray wavelength, $\theta$ is the Bragg's angle and $\beta$ is the pure full width of the fraction line at half of the maximum capacity. The surface texture characteristics obtained from nitrogen adsorption isotherms were measured at −196 °C using a conventional volumetric apparatus. The specific surface area was obtained using the BET method. The samples were thermally degassed at 300 °C prior to the adsorption measurements. The micropore volume and the external surface area were obtained from the $t$-plot. For the $TiO_2$ and lanthanides/$TiO_2$ photocatalysts explored in this work, bandgap energy was estimated with the Kubelka–Munk method using diffuse reflectance spectra [31]. The modified Kubelka–Munk function was determined using Eq. (1). We measured the optical spectra of pure $TiO_2$ and Re/$TiO_2$. Diffuse reflectance ultraviolet/visible spectra, plotted as the Kubelka–Munk function ($F$) of the reflectance, $R$(See supporting information S2). We introduced the $R$ value into the following equation.

$$\left(\frac{(1-R)^2}{2R}\times h\nu\right)^{1/2} \quad (1)$$

where $R$ is the proportion reflected, $h$ is Planck's constant, and $\nu$ is the frequency of light. Plots of this parameter were used to determine bandgap energy by determining a linear model for the linear portion of the absorption transition using least squares regression and extrapolating to zero at the corresponding photon energy [31].

### 2.4. Photocatalytic test

The photodegradation experiments were carried out by dissolving pure DB53 dye in water at the desired concentration (dye conc. = 100 ppm, pH ∼7; unless otherwise stated). The solution was adjusted at pH 2 (by using 0.2 M HCl), pH 4 (by using 0.2 M $CH_3COOH/CH_3$–COONa), and pH 7–9 (by using 0.2 M NaOH). The photocatalytic test composite is loaded between the cylinders and held in place by two screens of the desired mesh (See supporting information S1). The ends of the reactor are sealed by two Teflon end caps with inset O-rings. Contaminated water (grey water) is pumped through the media via Teflon inlet and outlet tubes. Several cooling ports are drilled through the Teflon covers to provide air cooling to the lamp. After homogenization by magnetic stirring, the sample was withdrawn via pump in the flow rate to get the retention time of 5–60 min. There is an inlet and outlet of the treated sample. The cells were exposed to xenon lamp at 150 W and $\lambda > 320$ nm. In the continuous recirculation mode experiments, aliquots (5 mL) were retrieved from the reservoir at certain time intervals and analyzed after filtering with a Millipore filter (0.2 mm). The concentration of the unreacted DB53 dye was analyzed with UV JASCO (V 570). The removal % of DB53 dye was measured by applying the following equation.

$$\text{Removal}\,\% = \frac{(C_o - C)}{C_o}\times 100 \quad (2)$$

where $C_o$ and $C$ are the initial concentration of DB53 and its remaining concentration in solution after reaction.

## 3. Results and discussions

### 3.1. Characterization of synthesized material

The crystalline phase of each parent $TiO_2$ and lanthanide ions-doped $TiO_2$ nanoparticles prepared by sol–gel was determined by XRD (Fig. 1). In parent titania and all lanthanide ions/$TiO_2$ photocatalysts, the figure presents a group of lines at $2\theta$ values of 25.2°, 37.5°, 47.7°, 53.3°, 54.7° and 62° which are attributed to anatase phase. No diffraction peaks of lanthanide oxides in the patterns of lanthanide ions/$TiO_2$ doped samples were observed. This is probably due to the low lanthanide ions doping content ∼1% and the data may also

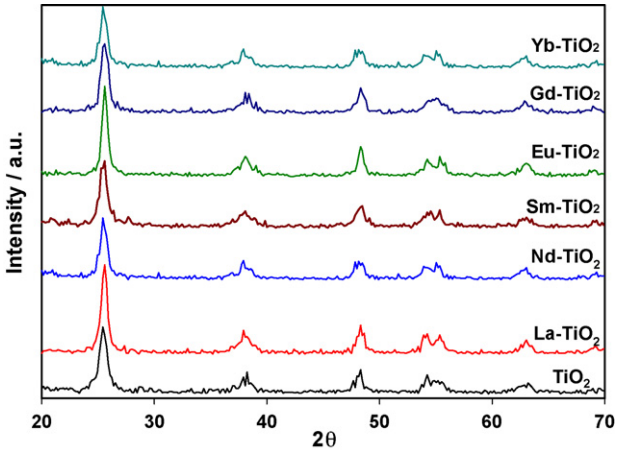


**Fig. 1.** XRD patterns of parent $TiO_2$ and RE–$TiO_2$ nanoparticles.

**Table 1**
Effect of type of lanthanides ions on crystallite size and bandgap of photocatalysts and dye removal efficiency.

| Sample | Crystallite size (nm) | Bandgap (eV) | Removal efficiency (%) |
|---|---|---|---|
| $TiO_2$ | 29.5 | 3.27 | 86 |
| La–$TiO_2$ | 22.1 | 3.12 | 89.9 |
| Nd–$TiO_2$ | 22.6 | 3.25 | 86.4 |
| Sm–$TiO_2$ | 21.9 | 3.26 | 87.3 |
| Eu–$TiO_2$ | 23.4 | 3.12 | 90 |
| Gd–$TiO_2$ | 20.3 | 3.11 | 91.5 |
| Yb–$TiO_2$ | 28.9 | 3.14 | 89.8 |

imply that, the lanthanide oxides are well dispersed within the $TiO_2$ phase. The XRD data revealed that all the studied lanthanide ions inhibit the phase transformation from anatase to rutile during calcinations even at high temperatures (550 °C) while in other works, the anatase phase started to convert into rutile before 500 °C [32]. The crystallite size, calculated from Scherrer equation ($D$) of pure $TiO_2$ and lanthanide ions/$TiO_2$ is summarized in Table 1. The crystallite size value is ranging from 20.3 to 29.5 nm at $2\underline{\theta} = 25.2^\circ$; the lanthanide/$TiO_2$ is lower crystallite size than $TiO_2$. This reduction in crystallite size is proposed due to segregation of the dopant cations at the grain boundary which inhibits the grain growth by restricting direct contact of grains [15]. The ionic radii of $Ti^{4+}$ is much smaller than those of lanthanide ions ($r$ for $Ti^{4+}$ = 0.68 Å, whereas $r$ for $La^{3+}$, $Nd^{3+}$, $Sm^{3+}$, $Eu^{3+}$, $Gd^{3+}$ and $Yb^{3+}$ = 1.032, 0.983, 0.958, 0.947, 0.938 and 0.868 Å, respectively [33]. From forgoing data $Ti^{4+}$ may substitute for lanthanide oxides in the lattice of rare earth oxides to form tetrahedral Ti sites. The interaction between the different tetrahedral Ti atoms or between the tetrahedral Ti and octahedral Ti inhibits the phase transformation to rutile [19].

The SEM photographs of the photocatalysts is shown in Fig. 2. The pure $TiO_2$ sample (A) and lanthanide ions-doped $Gd_2O_3/TiO_2$ (B) and $Yb_2O_3$–$TiO_2$ (C) showed relatively uniform with little defects in the indicating the excellent ordering of the photocatalyst samples. In addition, there is no change in the morphology after adding lanthanide ions that might be attributed to the lanthanide oxides are well dispersed within the $TiO_2$ phase.

The bandgap plays a critical role in deciding the photocatalytic activity of photocatalysts for the reason that it participates in determining the $e^-/h^+$ recombination rate. It was estimated by the diffuse reflectance absorption spectrum (See supporting information S2) and summarized in Table 1. It was clearly seen that, lanthanides ions-doped titania has a great advantage specifically in the decrease in bandgap of $TiO_2$, which has a pronounced effect of the semiconduction properties of the prepared nanoparticles. It has been established that anatase crystallites of this size exhibit

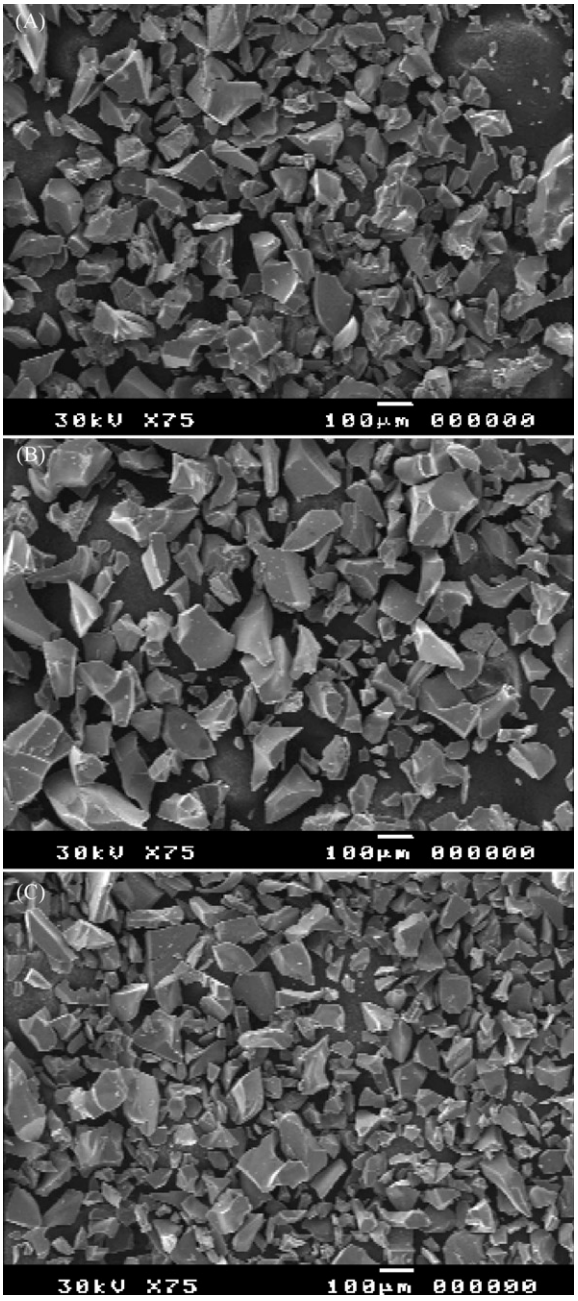


**Fig. 2.** SEM surface morphology of (a) $TiO_2$, (b) $Gd_2O_3/TiO_2$ and (c)$Yb_2O_3/TiO_2$.

bulk physical properties when the particle diameters are larger than 5 nm [34,35].

The obtained nitrogen adsorption–desorption isotherms for the $TiO_2$ and lanthanide ions-doped $TiO_2$ samples are typical of type II of Brunauer's classification with a small hystresis loop. The hystresis loop indicates the presence of porosity on the surface of the studied samples. The surface area, texture parameters calculated from the $t$-plot were estimated by the low-temperature nitrogen adsorption at relative pressures ($P/P_0$) in the range of 0.05–0.9 and are summarized in Table 2. An increase in the adsorption capacity of the $TiO_2$ was observed after introducing lanthanide ions. The surface area of Gd/$TiO_2$ was changed from 223 to 390 $m^2/g$ (~75% increase of surface area compared to the parent $TiO_2$). It is worth to mention that, the $S_{BET}$ values of the prepared photocatalysts are relatively higher than that of other analogues samples as mentioned in literature [36], Table 2. Furthermore, the total pore volume of lan-

**Table 2**
Textural parameters[a] of the lanthanides doped $TiO_2$ nanostructured.

| Sample | $S_{BET}$ ($m^2$/g) | $S_t$ ($m^2$/g) | $S_{mic}$ ($cm^2$/g) | $S_{meso}$ ($cm^2$/g) | $S_{ext}$ ($cm^2$/g) | $V_p$ ($cm^3$/g) | $V_{mic}$ ($cm^3$/g) | $V_{mes}$ ($cm^3$/g) | $r$ (Å) |
|---|---|---|---|---|---|---|---|---|---|
| $TiO_2$ | 223 | 363 | 21 | 201 | 23 | 0.193 | 0.184 | 0.009 | 21.67 |
| La–$TiO_2$ | 349 | 360 | 63 | 285 | 34 | 0.392 | 0.313 | 0.079 | 28.14 |
| Nd–$TiO_2$ | 312 | 244 | 24 | 287 | 12 | 0.224 | 0.194 | 0.029 | 17.97 |
| Sm–$TiO_2$ | 341 | 368 | 80 | 260 | 24.1 | 0.413 | 0.352 | 0.060 | 30.28 |
| Eu–$TiO_2$ | 367 | 368 | 66 | 300 | 36 | 0.406 | 0.321 | 0.085 | 27.71 |
| Gd–$TiO_2$ | 390 | 416 | 81 | 308 | 30 | 0.425 | 0.35 | 0.071 | 27.27 |
| Yb–$TiO_2$ | 331 | 337 | 57 | 273 | 26 | 0.355 | 0.297 | 0.058 | 26.87 |

[a] $S_{BET}$, BET-Surface area; $S_t$, surface area derived from $V_{l-t}$ plots; $S_{mic}$, surface area of micropores; $S_{mes}$, surface area of micropores; $S_{ext}$, external surface area; $V_p$, total pore volume; $V_{mic}$, pore volume of micropores; $V_{mes}$, pore volume of mesopores and $r^-$, mean pore radius.

thanide oxides–$TiO_2$ was twice that of $TiO_2$. Since the $TiO_2$ (anatase) structure is not affected by doping with lanthanide ions as revealed by XRD, the increase of surface area and mesopore volume was observed for the lanthanide ions-doped $TiO_2$. In turn, further data assessment reveals that, the values of $S_{BET}$ and $S_t$ are generally close in most samples indicating the presence of mesopores. The values of external surface area ($S_{ext}$) of the samples are very small which verifies the porous nature of these solids. The values of $S_{meso}$ are high compared to that of $S_{micro}$ implying that the main surface is mesoporous solid as represented by the isotherm. The surface texture data will be correlated with the catalytic activity as will be mentioned later on.

### 3.2. Photocatalytic activity studies

The photodegradation of DB53 dye was used as a probe reaction to test the photocatalytic activity of the prepared lanthanide ions/titania nanoparticles. Fig. 3 shows the effect of lanthanide oxides/titania nanoparticles on photocatalytic degradation of DB53 dye [100 ppm] after 30 min at 25 °C at pH 7.7 and 0.25 g/L loading catalyst. The data presents that the photocatalytic activities of the lanthanide ions-doped titania nanoparticles is higher than that of parent $TiO_2$. Knowing that, the pure lanthanide oxides do not have photocatalytic oxidation properties, such variation in activity must be due to the differences in interaction between lanthanide ions oxides and $TiO_2$. That led to several modifications in physical properties such as bandgap, particle size and surface texture. The photocatalytic activity of titania generally increased with the addition of lanthanide ions promoters. It is clearly seen that Gd/$TiO_2$ as a photocatalyst is highly photoactive than other pure titania and lanthanides ions. Our results are in good agreement with reference [17].

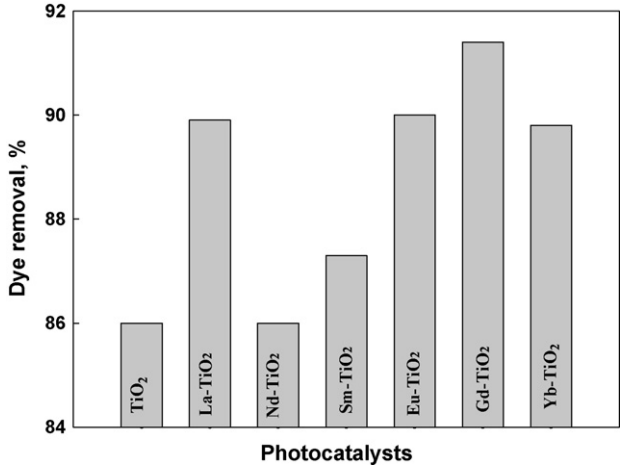


**Fig. 3.** Effect of lanthanide ion-doped $TiO_2$ on the photodegradation of DB53. Photocatalyst loading, 0.25 g/L; [100 ppm] DB53 dye ($O_2^-$ saturated, pH 7.7, $T$ = 25 °C), illumination time 30 min.

$La^{3+}$, $Nd^{3+}$, $Sm^{3+}$, $Eu^{3+}$, $Gd^{3+}$ and $Yb^{3+}$/$TiO_2$, as mentioned before, $Ti^{4+}$ may replace the lanthanide oxides with a trivalent oxidation state and creates a charge imbalance. The charge imbalance must be stated; therefore more hydroxide ions would be adsorbed on the surface for charge balance. These hydroxide ions on the surface can accept holes generated by UV illumination to form hydroxyl radicals, which oxidize adsorbed molecules and therefore decrease the $e^-/h^+$ recombination rate (see Eqs. (3)–(9)). Previous studies have proposed that $^\bullet OH$ and $H_2O_2$, derived from water or surface hydroxyls through photooxidation, are involved in the photooxidation organic compounds [37].

$$Ti^{IV}ORE^{III} + h\nu \rightarrow \{Ti^{III}OH\} + \{RE^{IV}OH^\bullet\}^+ \quad (3)$$

$$\{RE^{IV}OH^\bullet\}^+ + OH^- \rightarrow {}^\bullet OH + RE^{III}OH \quad (4)$$

$$\{Ti^{III}OH\} + O_2 \rightarrow \{Ti^{IV}OH\} + O_2{}^{-\bullet} \quad (5)$$

$$O_2{}^{-\bullet} + H^+ \rightarrow HO_2{}^\bullet \quad (6)$$

$$HO_2{}^\bullet + \{Ti^{III}OH\} \rightarrow HO_2{}^- \quad (7)$$

$$HO_2{}^- + H^+ \rightarrow H_2O_2 \quad (8)$$

$$C_{34}H_{24}N_6Na_4O_{14}S_4 + 47O_2 + H_2O \rightarrow 34CO_2 + 6NO_3{}^- + 4SO_4{}^{2-} + 4Na^+ + 12H^+ + 7H_2O \quad (9)$$

It is clear that, the photocatalytic activity of Gd/$TiO_2$ was the highest due to it has high surface area and pore volume and low bandgap (see Fig. 3 and Tables 1 and 2). The results show that the photocatalytic activities of lanthanide ions-doped titania nanoparticles increased with decreasing the bandgap values (See Table 1). This is due to the energy ($h\nu$) required is direct proportional with bandgap and hence decrease the energy needed to excite electron from valance band to conduction band. The high activity of Gd/$TiO_2$ dopants may also be related to its half filled ($t$) electronic configuration.

#### 3.2.1. Effect of pH on the photodegradation of DB53 dye

Fig. 4 shows the effect of pH of Direct Blue dye on its photocatalytic oxidation over Gd–$TiO_2$ after 30 min illumination time using the previous stated reaction conditions. The findings were revealed that the increase of pH value of dye solution from 2 to 4 let to slightly increase of dye removal ~0.5% and then dye removal decreased to 82.7 at pH 9 (Fig. 4). This is interpreted that, DB53 dye has negative charge, whereas lanthanide ions–$TiO_2$ has positive charge in acidic medium. Consequently, the increase in pH value tended to change the charge on lanthanide ions–$TiO_2$ to negative charge and in turn, the dye removal decreased due to the repulsion between lanthanide oxides–$TiO_2$ and anionic dye [38]. In addition, the increase of pH may increase the rate of $e^-/h^+$ recombination rate and thus decreases the photocatalytic activity. Therefore, the optimum pH value for the photodegradation of DB53 dye is ~4 at which photocatalytic oxidation is being maximum.

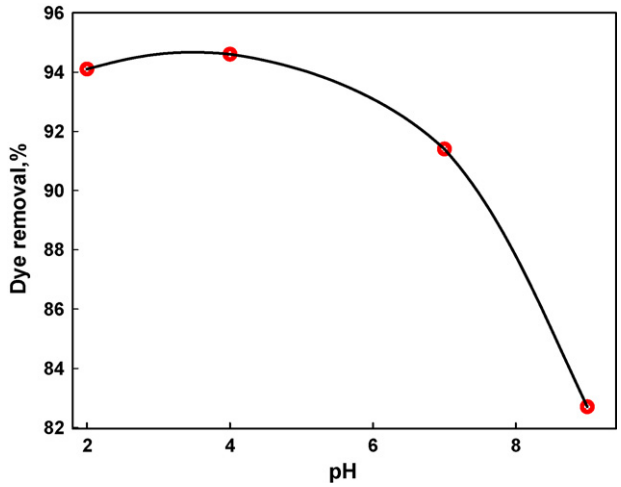


**Fig. 4.** Effect of pH on the photodegradation of DB53 using Gd–$TiO_2$ photocatalyst. Photocatalyst loading, 0.25 g/L; [100 ppm] DB53 dye ($O_2^-$ saturated, $T$ = 25 °C), illumination time 30 min.

### 3.2.2. *Effect of reaction time on the photodegradation of DB53 dye*

About 60% of DB53 dye (100 ppm) was photodegraded on the surface of Gd–$TiO_2$ after 5 min as shown in Fig. 5. The remained dye was completely oxidized within 40 min. Such data reveals the relative high activity of the prepared photocatalysts which enables the complete degradation of the pollutant in such short time and the photocatalyst have active sites to carry out the reaction.

### 3.2.3. *Effect of photocatalyst loading on the photodegradation of DB53 dye*

The results show that the increment of photocatalyst loading from 0.1 to 0.4 g/L increased the dye removal % from 75% to 100%, respectively Fig. 6. With increasing the weight above 0.4 g/L, the photoactivity decreased [39,40]. The reasons for this decrease in degradation rate were aggregation of lanthanide ions/$TiO_2$ particles at high concentration causing a decrease in the number of surface active sites and increase the opacity and light scattering of lanthanide oxides–$TiO_2$ particles at high concentration. This tends to decrease the passage of irradiation through the sample [41]. On other hand, the findings indicated that there was slightly increase of dye removal ~1.5% by increasing photocatalyst loadings from 0.3 to 0.4 g/L, therefore, from economic point of view, the optimized photocatalyst loading is 0.3 g/L.

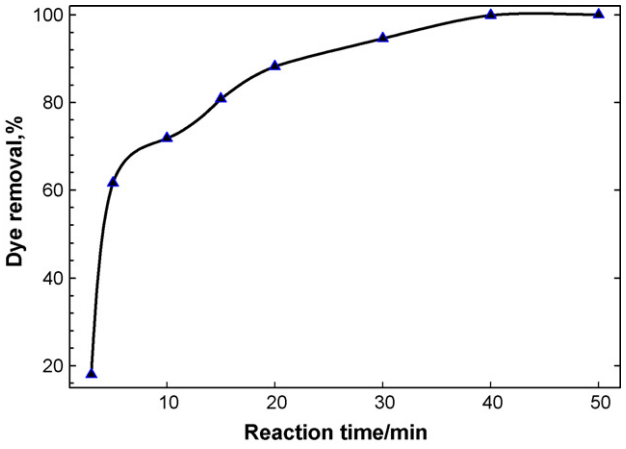


**Fig. 5.** Effect of reaction time on the photodegradation of DB53 using Gd–$TiO_2$ photocatalyst. Photocatalyst loading, 0.25 g/L; [100 ppm] DB53 dye ($O_2^-$ saturated, pH 4, $T$ = 25 °C),.

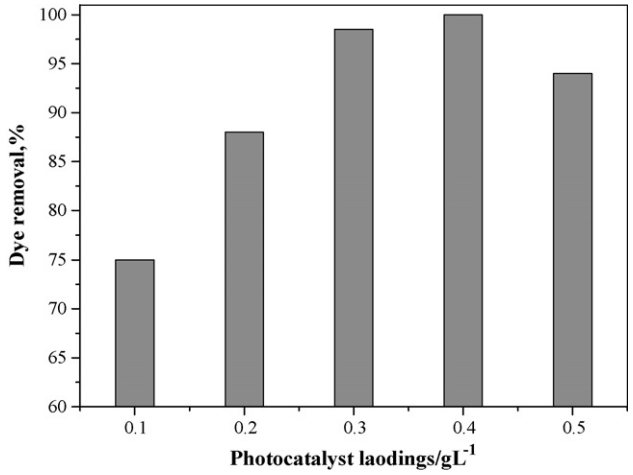


**Fig. 6.** Effect of loading of Gd–$TiO_2$ photocatalyst on the photodegradation of DB53. [100 ppm] DB53 dye ($O_2^-$ saturated, pH 4, $T$ = 25 °C), illumination time 40 min.

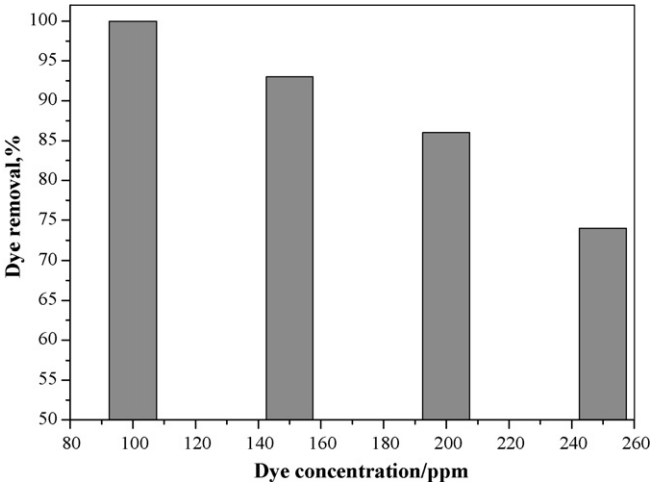


**Fig. 7.** Effect of the initial concentration of DB53 on the the photodegradation of DB53 using Gd–$TiO_2$ photocatalyst. Photocatalyst loading, 0.3 g/L;($O_2^-$ saturated, pH 4, $T$ = 25 °C), illumination time 40 min.

### 3.2.4. *Effect of DB53 dye concentration*

The effect of the initial DB53 dye concentration on the photocatalytic oxidation was studied (Fig. 7). The results show that the increment of initial dye concentration from 100 to 250 ppm led to a decrease in the photocatalytic degradation of DB53 from 100% to 75.1%, respectively. The rate of degradation relates to the formation of hydroxyl radicals, which is the critical species in the degradation process. Hence an explanation to this behavior is that the higher the initial concentration, the higher adsorbed organic substances on the surface of lanthanide ions–$TiO_2$. In the same time the intensity of light and illumination are constant, so the path length of photons entering the solution decreases and in low concentration, the reverse effect is observed and consequently the $OH^•$ radicals formed on the surface of lanthanide ions–$TiO_2$ nanoparticles decrease. With decreasing the number of $OH^•$ radicals attacking the surface, the relative OH number attaching the compound decreases and thus the photo degradation efficiency decreases [40].

## 4. Conclusions

The sol–gel method is useful for the preparation of nanostructured lanthanide ions–$TiO_2$ with high photocatalytic activity, high surface area and desirable pore structures. A series of Nd,

Sm, Eu, Gd, Yb and La homogenously doped nanocrystalline $TiO_2$ has been successfully synthesized by sol–gel method. The type of dopant lanthanide ion showed significant effect on the texture structure, bandgap and particle size. These physical changes affected on the efficiency of the photodegradation of DB53 dye. The dye removal % is well correlated with the bandgap, surface area and pore volume. In addition, the differences in photoactivity are due to the change in the amount of surface hydroxyl groups resulting from the interaction between the rare earth oxides and $TiO_2$. The Gd–$TiO_2$ nanoparticles presented the highest dye removal % due to its high surface area, large pore volume, small particle size and small bandgap.

## Appendix A. Supplementary data

Supplementary data associated with this article can be found, in the online version, at doi:10.1016/j.jhazmat.2008.11.022.

## References


[1] P.C. Calza, et al., Single-step synthesis of a highly active visible-light photocatalyst for oxidation of a common indoor air pollutant: acetaldehyde, Adv. Mater. 17 (2005) 2467.
[2] H. Kisch, W. Macyk, Visible-light photocatalysis by modified titania, Chem. Phys. Chem. 3 (2002) 399.
[3] A.P. Davis, D.L. Green, Green photocatalytic oxidation of cadmium–EDTA with titanium dioxide, Environ. Sci. Technol. 33 (1999) 609.
[4] H. Choi, A.C. Sofranko, D.D. Dionysiou, Nanocrystalline $TiO_2$ photocatalytic membranes with a hierarchical mesoporous multilayer structure: synthesis, characterization, and multifunction, Adv. Funct. Mater. 16 (2006) 1067.
[5] A.P. Hong, D.W. Bahnemann, M.R. Hoffmann, Cobalt(II) tetrasuifophthalocyanine on titanium dioxide: a new efficient electron relay for the photocatalytic formation and depletion of hydrogen peroxide in aqueous suspensions, J. Phys. Chem. 91 (1987) 2109.
[6] H. Hidaka, Y. Asai, J. Zhao, K. Nohara, E. Pelizzetti, N. Serpone, Photoelectrochemical decomposition of surfactants on a $TiO_2$ particulate film electrode assembly, J. Phys. Chem. 99 (1995) 8244.
[7] L. Kruczynski, H.D. Gesser, C.W. Turner, E.A. Speer, Porous titania glass as a photocatalyst for hydrogen production from water, Nature 291 (1981) 399.
[8] N. Serpone, P. Maruthamuthu, E. Pelizzetti, H. Hidaka, Exploiting the interparticle electron transfer process in the photocatalysed oxidation of phenol, 2-chlorophenol and pentachlorophenol: chemical evidence for electron and hole transfer between coupled semiconductors, J. Photochem. Photobiol. A 85 (1995) 247.
[9] K.Y. Song, M.K. Park, Y.T. Kwon, H.W. Lee, W.J. Chung, W.I. Lee, Preparation of transparent particulate $MoO_3/TiO_2$ and $WO_3/TiO_2$ films and their photocatalytic properties, Chem. Mater. 13 (2001) 2349.
[10] A.A. Ismail, I.A. Ibrahim, R.M. Mohamed, H. El-Shall, Sol–gel synthesis of titania–silica photocatalyst for cyanide photodegradation, J. Photochem. Photobiol. A 63 (2004) 445.
[11] B. Pal, T. Hata, K. Goto, G. Nogami, Photocatalytic degradation of o-cresol sensitized by iron–titania binary photocatalysts, J. Mol. Catal. A: Chem. 169 (2001) 147.
[12] A.A. Ismail, Synthesis and characterization of $Y_2O_3/Fe_2O_3/TiO_2$ nanoparticles by sol–gel method, Appl. Catal. B: Environ. 58 (2005) 115.
[13] Y. Wang, H. Cheng, L. Zhang, Y. Hao, J. Ma, B. Xu, W. Li, The preparation, characterization, photoelectrochemical and photocatalytic properties of lanthanide metal-ion-doped $TiO_2$ nanoparticles, J. Mol. Catal. A 151 (2000) 205.
[14] Y. Zhang, H. Zhang, Y. Xu, Y. Wang, Significant effect of lanthanide doping on the texture and properties of nanocrystalline mesoporous $TiO_2$, J. Solid State Chem. 177 (2004) 3490.
[15] Y. Zhang, H. Xu, H. Zhang, Y. Wang, The effect of lanthanide on the degradation of RB in nanocrystalline Ln/$TiO_2$ aqueous solution, J. Photochem. Photobiol. A 170 (2005) 279.
[16] K.T. Ranjit, I. Willner, S.H. Bossmann, A.M. Braun, Lanthanide oxide-doped titanium dioxide photocatalysts: novel photocatalysts for the enhanced degradation of *p*-Chlorophenoxyacetic acid, Environ. Sci. Technol. 35 (2001) 1544.
[17] W. Xu, Y. Gao, H.-Q. Liu, The preparation, characterization, and their photocatalytic activities of rare-earth-doped $TiO_2$ Nanoparticles, J. Catal. 207 (2002) 151–157.
[18] J. lin, J.C. Yu, An investigation on photocatalytic activities of mixed TiO, -rare earth oxides for the oxidation of acetone in air, J. Photochem. Photobiol. A 116 (1998) 63.
[19] D.W. Hwang, J.S. Lee, W. li, S.H. Oh, Electronic band structure and photocatalytic activity of $Ln_2Ti_2O_7$ (Ln) La, Pr, Nd), J. Phys. Chem. B 107 (2003) 4963.
[20] Y.H. Zhang, H.X. Zhang, Y.X. Xu, Y.G. Wang, Europium doped nanocrystalline titanium dioxide: preparation phase transformation and photocatalytic properties, J. Mater. Chem. 13 (2003) 2261.
[21] J. Lin, J. Yu, S.K. Lam, Photocatalytic activity of rutile $Ti_{1-x}Sn_xO_2$ solid solutions, J. Catal. 183 (1999) 368.
[22] R. Gopalan, Y.S. Lin, Evolution of pore and phase structure of sol–gel derived lanthana doped titania at high temperatures, Ind. Eng. Chem. Res. 34 (1995) 1189.
[23] G. Boschloo, A. Hagfeldt, Photoinduced absorption spectroscopy of dye-sensitized nanostructured $TiO_2$, Chem. Phys. lett. 370 (2003) 381.
[24] A. Xu, Y. Gao, H. Liu, The Preparation, Characterization, and their photocatalytic activities of rare-earth-doped $TiO_2$ nanoparticles, J. Catal. 207 (2002) 151.
[25] M.S.P. Francisco, V.R. Mastelaro, Inhibition of the anatase-rutile phase transformation with addition of $CeO_2$ to CuO–$TiO_2$ system: Raman spectroscopy, X-ray diffraction, and textural studies, Chem. Mater. 14 (2002) 2514.
[26] C.P. Sibu, K.S. Rajesh, P. Mukundan, K.G.K. Warrier, Structural modifications and associated properties of lanthanum oxide doped sol–gel nanosized, Chem. Mater. 14 (2002) 2876.
[27] H. Zollinger, in: H.F. Ebel, C.D. Brenzinger (Eds.), Color Chemistry, 1st ed., VCH, New York, 1987 (Chapter 16).
[28] W.G. Kuo, Decolorizing dye wastewater with Fenton's reagent, Water Res. 26 (1992) 881.
[29] N.I. Sax, Cancer Causing Chemical, 1st ed., DC 9625000, VNR New York, 1981.
[30] P. Klug, L.E. Alexander, Direction Procedures for Polycrystalline and Amorphous Materials, Wiley, 1954.
[31] W.Y. Teoh, R. Amal, L. Madler, S.E. Pratsinis, Flame sprayed visible light-active Fe–TiO2 for photomineralisation of oxalic acid, Catal. Today 120 (2007) 203.
[32] K.Y. Jung, S.B. Park, Anatase-phase titania: preparation by embedding silica and photocatalytic activity for the decomposition of trichloroethylene, J. Photochem. Photobiol. A Chem. 127 (1999) 117.
[33] R.D. Shannon, Acta Crystallogr. A 32 (1976) 751.
[34] C. Kormann, W.D. Bahnemann, R.M. Hoffmann, Preparation and characterization of quantum-size titanium dioxide, J. Phys. Chem. 92 (1988) 5196.
[35] S. Monticone, R. Tufeu, V.A. Kanaev, E. Scolan, C. Sanchez, Quantum size effect in $TiO_2$ nanoparticles: does it exist? Appl. Surf. Sci. 162–163 (2000) 565.
[36] P. Yang, C. Lu, N. Hua, Y. Du, Titanium dioxide nanoparticles co-doped with $Fe^{3+}$ and $Eu^{3+}$ ions for photocatalysis, Mater. Lett. 57 (2002) 794.
[37] M.R. Hoffmann, S.T. Martin, W. Choi, D.W. Bahnemann, Environmental applications of semiconductor photocatalysis, Chem. Rev. 95 (1995) 69–96.
[38] C.A. Le Duc, J.M. Campbell, J.A. Rossin, Effect of Lanthana as a stabilizing agent in Titanium dioxide support, Ind. Eng. Chem. Res. 35 (1996) 2473.
[39] D. Chen, A.K. Ray, Photodegradation kinetics of 4-nitrophenol in $TiO_2$ suspension, Water Res. 32 (1998) 3223.
[40] A. mills, S. Morris, Photomineralization of 4-chlorophenol sensitized by titanium dioxide: a study of the initial kinetics of carbon dioxide photogeneration, J. Photobiol. A: Chem. 71 (1993) 75.
[41] A.P. Toor, A. verma, C.K. Jotshi, P.K. Bajpai, V. singh, Photocatalytic degradation of Direct Yellow 12 dye using UV/$TiO_2$ in a shallow pond slurry reactor, Dyes Pigments 68 (2006) 53.